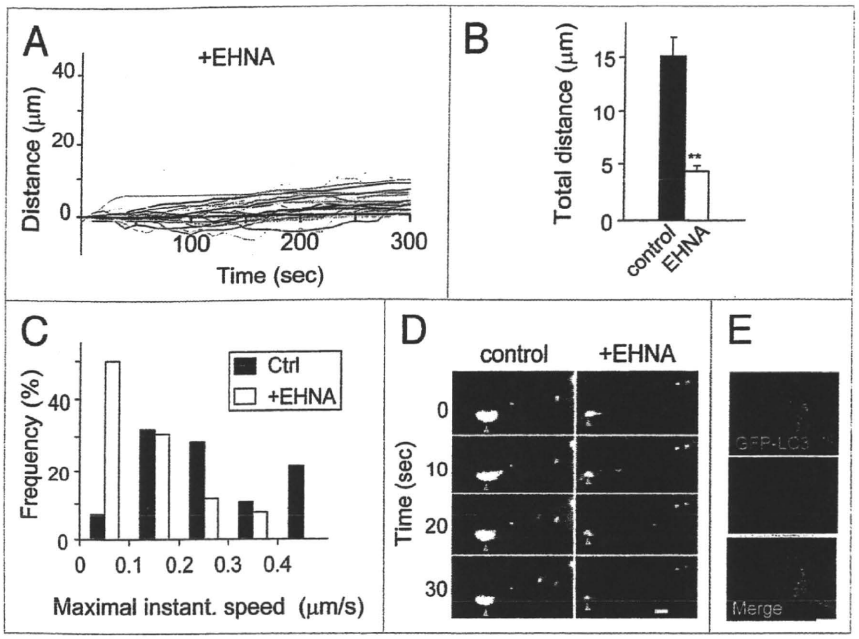

Figure 3. EHNA treatment inhibited the movement of autophagosomes in axons. (A) Kymographs of autophagosomes following EHNA treatment. After treating the GFP-LC3 granule cells with EHNA (50 μM) for 4 h, the positions of 26 autophagosomes in the axons were recorded every 10 s and plotted against time. (B) Total distance that the autophagosomes travelled in control and EHNA-treated granule cell axons during 5-min periods. (C) Frequency histogram of the maximal instantaneous speed of autophagosomes per frame. The maximal instantaneous speed at which each autophagosome moved during the 5-min observation period in control and EHNA-treated granule cell axons was plotted. **$p < 0.01$. (D) Representative time-lapse images of DsRed-tagged synaptophysin in axons of granule cells. Cerebellar explant cultures were infected with lentivirus encoding DsRed-synaptophysin at 7 DIV and imaged at 14 DIV after treatment with or without EHNA for 4 h. Red arrows indicate DsRed-synaptophysin fluorescence and blue arrowheads indicate synaptic buttons. Scale bar, 1 μm. (E) Colocalization of GFP-LC3 dots with putative lysosomes in the soma of granule cells. *GFP-LC3* granule cells were fixed and double-immunostained for a lysosomal marker lamp-1 (red) and GFP-LC3 (green).

treated granule neurons ($p < 0.01$ according to the Mann Whitney *U* test; **Fig. 4A**). Time-lapse imaging of the GFP-LC3 dots in the axons revealed that the population of fast-moving autophagosomes tended to increase in the axons of NMDA-treated neurons (**Fig. 4B**), although most autophagosomes moved relatively slowly in both NMDA-treated and control neurons; thus, the mean distances that the autophagosomes traveled did not differ significantly between these two groups (**Fig. 4C**). Similarly, the maximal speed at which each autophagosome moved during the 5-min observation periods peaked at 0.4–0.5 μm/s in neurons treated with NMDA, while it peaked at 0.2–0.3 μm/s in the control neurons (**Fig. 4D**), although the mean velocity did not differ significantly between these two groups (0.36 ± 0.03 μm/s for NMDA vs. 0.27 ± 0.03 μm/s for control, $p > 0.1$ according to the Mann-Whitney *U* test). Thus, although whether NMDA treatment increased the overall trafficking of autophagosomes remains unclear, it seemed to stimulate the movement of at least a proportion of the autophagosome population. These results indicate that excitotoxic stimuli, as mimicked by NMDA treatment, increased the number of autophagosomes in axons not by inhibiting their movements.

Finally, to further examine whether NMDA treatment increased the de novo formation of autophagosomes, we performed immunoblotting analysis with anti-LC3 antibody; a lipidated form of LC3, LC3-II, has been shown to be a specific autophagosomal marker in mammals.[27] We found that the ratio of LC3-II to its unlipidated form LC3-I was significantly increased in lysates prepared from cultured granule cells treated with 300 μM of NMDA plus 5 μM of glycine for 24 h ($p < 0.05$, $n = 5$; **Fig. 5A and B**). When fusion of autophagosomes and lysosomes was blocked by incubation with a medium containing 200 nM of bafilomycin A1 (BafA)[28] for the last 4 h, the LC3-II/LC3-I ratio was significantly increased in both control and NMDA-treated granule cells ($p < 0.01$ vs. control without BafA, $n = 5$; **Fig. 5A and B**). Importantly, the LC3-II/LC3-I ratio was significantly higher in NMDA/BafA-treated cells than in NMDA-treated cells ($p < 0.01$, $n = 5$; **Fig. 5A and B**), a result indicating that NMDA-induced increase in the LC3-II/LC3-I ratio was caused by enhancement of the autophagic influx, not by inhibition of autophagic degradation.[29,30] Furthermore, the level of p62/SQSTM1, a selective substrate of autophagy used as an indicator of autophagic degradation activity,[31] was reduced by NMDA treatment (**Fig. 5C**). These results are consistent with increased GFP-LC3 dots in axons of granule cells (**Fig. 4**) and support the view that NMDA treatment increased the de novo formation of autophagosomes in granule cells.

Discussion

Although the accumulation of autophagosomes within axons is often observed in axonopathies associated with various neurological disorders, the life cycle of autophagosomes in axons is not well understood.[10,11] In the present study, we used microexplant cultures of cerebellar granule cells from GFP-LC3 transgenic mice to perform time-lapse imaging of LC3-positive autophagosomes in well-defined CNS axons.

Dynamics of autophagosomes in axons under physiological conditions. The basal autophagic activity level is generally considered very low in the brain in vivo.[5,6] Nevertheless, we constantly observed a small number of GFP-LC3 dots in the axons of cultured granule cells under normal conditions. This result might be explained by the difficulty that arises when using the thin slices required for an electron microscopic analysis to detect the small number of autophagosomes in long axons running in various directions. In addition, since the granule cells that were used in this study correspond to those at early developmental stages (postnatal days 10–14), the endogenous autophagic activity level might have been relatively high.[32] Also, the autophagic

activity level might have been somewhat increased because of the culture conditions, under which some nutrients were missing. Nevertheless, few autophagosome-like double membrane structures have been reported in the axons of wild-type Purkinje cells neurons in vivo.[7,33] In addition, the earliest sign of neurodegeneration in neuron-specific *Atg5* or *Atg7* knockout mice is a local swelling of the axons around their terminals,[7,8] indicating that autophagic activity plays crucial physiological roles in the maintenance of axons. Therefore, we believe that the dynamics of autophagosomes observed in cultured granule cells at least partly reflect those naturally occurring in vivo.

Microtubules are arranged in axons so that each minus end points toward the nucleus. Dynein is the major minus-end motor that transports various cargos on microtubules. Since the movement of the autophagosomes in the axons was greatly reduced by the dynein motor inhibitor EHNA (**Fig. 3A–C**), the autophagosomes likely traveled preferentially in a retrograde direction via dynein motors. Autophagosomes were previously reported to undergo bidirectional transport in neurites following the deprivation of a nerve growth factor in SCG neurons and PC12 cells.[18] The reason why autophagosomes did not show vectorial movement in neurites (a mixture of axons and dendrites) of SCG neurons and PC12 cells is unclear, but microtubules may be arranged differently in neurites than in axons. In contrast, GFP-LC3 reportedly exhibited unidirectional, retrograde transport in putative axons of cerebellar granule cells in dissociated cultures when examined in a preliminary study.[19] Although the details were not described, small antegrade movement could be easily missed if time-lapse imaging was performed for a short duration or at long intervals. Recently, autophagosomes have been shown to travel bidirectionally with a net movement towards the microtubule-organizing center in HeLa cells[34] and rat kidney cells.[35] Furthermore, the movement of autophagosomes and its fusion with lysosomes, which are located around the centrosome, was also reduced by EHNA and other reagents blocking dynein motors in these cells.[34,35] Therefore, the present study has not only confirmed earlier studies reporting that autophagosomes show dynamic movements in neurons, but has also established the view that autophagosomes undergo bidirectional transport with a bias towards the soma, where most lysosomes are located (**Fig. 3D**), in the CNS axons as well as in other non-neuronal cells.

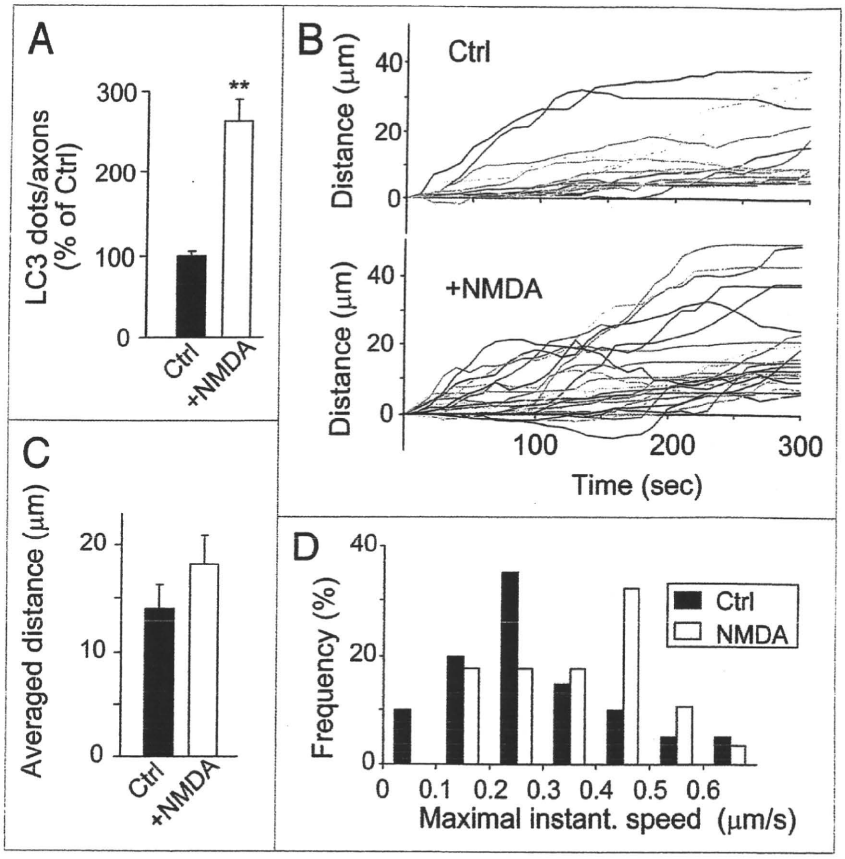

Figure 4. Activity-dependent regulation of autophagosomes in granule cell axons. (A) Increased number of autophagosomes in the axons of granule cells treated with NMDA. The number of GFP-LC3 dots per unit length in randomly selected distal axons was counted in granule cells treated with NMDA (300 μM) plus glycine (5 μM) for 24 h. The value in control granule cells treated with APV (50 μM) was arbitrarily defined as 100%. **$p < 0.01$, $n = 30$ regions each. (B) Kymographs of autophagosomes in control and NMDA-treated granule cells. After treating GFP-LC3 granule cells with NMDA or APV (control) for 24 h, the positions of the autophagosomes (26 for control and 28 for NMDA) in the axons were recorded every 10 s and plotted against time. (C) Total distance that the autophagosomes traveled in control and NMDA-treated granule cell axons during 5-min periods. (D) Frequency histogram of the maximal instantaneous speed of autophagosomes per frame. The maximal instantaneous speed at which each autophagosome moved during the 5-min observation period in control and NMDA-treated granule cell axons was plotted.

Autophagosomes under pathological conditions. The application of NMDA[15,16] or kainate[36] to neurons reportedly results in an increase in the number of autophagosome-like structures and the accumulation of the lipidated form of LC3, which is associated with autophagosomal membranes, in neurons. Although the mechanisms underlying this phenomenon are still unclear, either an enhancement in the de novo formation of autophagosomes or a decrease in the clearance of existing autophagosomes might be responsible. For example, the decreased clearance of autophagosomes is associated with several neurodegenerative disorders, such as Alzheimer disease[12] and Parkinson disease.[14] In contrast, in *lurcher* mutant mice, where a constitutive activity of the δ2 glutamate receptor causes the neurodegeneration of cerebellar Purkinje cells,[37,38] the earliest sign of abnormality was the accumulation of autophagosomes in Purkinje cell axons without a reduction in the clearance of autophagosomes.[39] Recently, autophagosome formation in *lurcher* have been shown to be caused by excessive cation influx into Purrkinje cells.[40] The present findings that NMDA treatment increased the number of GFP-LC3 dots in axons (**Fig. 4**) and enhanced the de novo formation of autophagosomes (**Fig. 5**) also support the view that

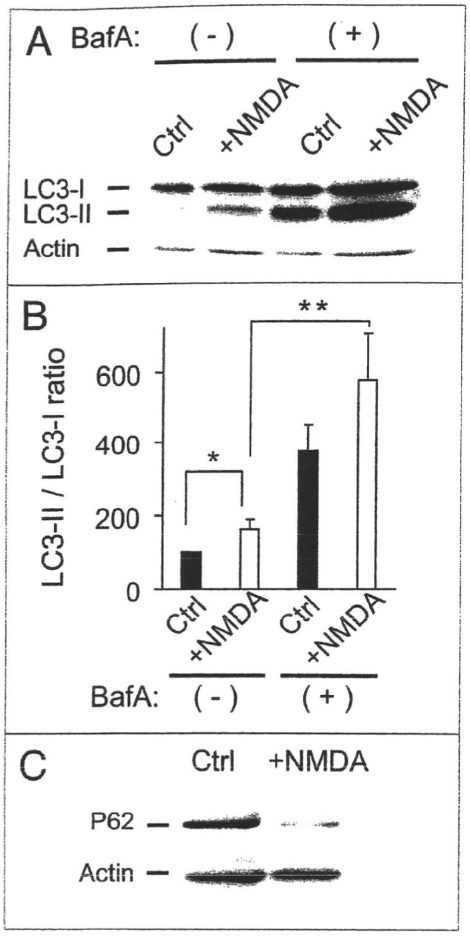

Figure 5. The effect of NMDA treatment on the production and degradation of autophagosomes. (A and B) Cultured granule cells were treated with 50 μM APV (Ctrl) or 300 μM NMDA plus 5 μM glycine (+NMDA) for 24 h. The cells were treated with (+) or without (-) 200 nM bafilomycin A1 (BafA) for the last 4 h and subjected to immunoblot analysis using anti-LC3 and anti-actin antibodies. Representative images (A) and quantitative analysis (B) were shown. The actin level was shown as a control. Each bar represents the mean + SEM (n = 5) *$p < 0.05$, **$p < 0.01$. (C) Immunoblot analysis of granule cells treated with NMDA using anti-p62/SQSTM1 antibody. The p62/SQSTM1 level was reduced in granule cells treated with 300 μM NMDA plus 5 μM glycine (+NMDA) for 24 h, a result indicating an increased autophagic activity. The actin level was shown as a control.

excitotoxic insults, which accompany cation influx, induce the formation of autophagosomes in axons.

Although the maximal movement of the autophagosomes in the axons (0.07–0.49 μm/s; **Fig. 2D**) was slower than what can be achieved using dynein motors (1–4 μm/s),[41] it was similar to that observed in rat kidney cells (0.05–0.24 μm/s).[35] Similarly, although the responsible motors are unclear, ER subcompartments and RNA granules have been shown to travel bidirectionally in the dendrites of hippocampal neurons at speeds of 0.2–0.3 μm/s.[42] The slow movement of autophagosomes observed in axons may result from the occurrence of intermittent pauses or directional switching. Thus, if the formation of autophagy is further increased under pathological conditions in neurons that have long axons, the slow speed of the retrograde movement could become the rate-limiting step of the turnover of autophagosomes. Indeed, the loss of dynein function reportedly causes neurodegeneration by reducing the rate of the autophagic clearance of misfolded proteins.[43] Interestingly, although lysosomes are mainly located near the nucleus of neurons under normal conditions, they were also observed in the axons of *lurcher* Purkinje cells,[39] suggesting that under some conditions, lysosomes may be formed at or transported to axons and may help the clearance of autophagosomes locally. Further studies are warranted to clarify the mechanisms by which the number and movement of autophagosomes and lysosomes are controlled in axons under physiological and pathological conditions.

Materials and Methods

Animals. *GFP-LC3* transgenic mice (B57BL/6J) were generated as described previously[17] and crossed with neural cell-specific *Atg5* deficient mice (*Atg5*$^{flox/flox}$; nestin-*Cre*, 129xB57BL/6J).[5] Genotyping for the *GFP-LC3*, *Atg5*^{flox} and the *Cre* gene has been described previously.[5,17] ICR mice were purchased from SLC (Hamamatsu, Japan). All procedures relating to the care and treatment of the animals were performed in accordance with the NIH guidelines. The animals were killed by decapitation after anesthetization with tribromoethanol.

Virus preparation and cerebellar infection. The expression plasmid of pPDGF-synaptophysin-EGFP were kindly provided by Dr. Y. Goda (University College London, London, UK). The cDNA encoding EGFP in the plasmid was replaced by that of DsRed-Monomer (DsRed) (Clontech, 632466) and subcloned into pCL20cMSCV vector[44] to produce pCL20cMSCV-synaptophysin-DsRed. Vesicular Stomatitis Virus-G protein (VSV-G) pseudotyped lentiviral vectors were provided by St. Jude Children's Research Hospital (Memphis, TN, USA). Virus particles were produced according to the method described earlier.[45] Briefly, human embryonic kidney (HEK) 293T cells were transfected with a mixture of four plasmids, pCAGkGP1R, pCAG4RTR2, pCAG-VSV-G and pCL20cMSCV-synaptophysin-DsRed, by a calcium phosphate precipitation method. Sixteen hours after transfection, the cells were washed with phosphate-buffered saline (PBS) twice and then cultured for an additional 24 h. The medium containing virus particles was harvested 40 h after transfection, filtered and centrifuged at 25,000 rpm for 90 min. The virus particles were finally suspended in PBS (pH 7.4), frozen in aliquots, and stored at -80°C. The titers of virus stocks were measured by transducing HEK 293T cells. Cerebellar microexplant cultures were infected with lentivirus at 7 d in vitro and incubated for additional 7 d for live-cell imaging.

Cell cultures. Cerebellar microexplant cultures were prepared as described previously.[46] Briefly, the cerebella from 5- to 7-day-old *GFP-LC3* or *GFP-LC3*; *Atg5*$^{flox/flox}$; nestin-*Cre* transgenic mice were isolated, freed from meninges and the choroid plexus using fine forceps, and cut into small pieces (30–50 μm) with scissors in ice-cold Hanks' balanced salt solution (Nacalai Tesque, 17460-15). The microexplants were washed three times, plated on 18-mm coverslips (Fisher Scientific) coated with poly-L-ornithine hydro bromide (Sigma, P4638), and maintained at

37°C with 5% CO_2 in a serum-free culture medium consisting of Neurobasal medium (Invitrogen, 21103-049) supplemented with 2.5 mM L-glutamine (Nacalai Tesque, 16919-55), 2.5% B-27 (Invitrogen, 0050129SA), and 0.01% penicillin/streptomycin. The cultured cells were used for experiments at 5–7 days in vitro.

Primary cultures of cerebellar granule cells were prepared from ICR mice on postnatal day 5–7, as described previously.[47] Cells were plated at a density of 2 x 10^5 cells on 35 mm-diameter dishes. Cells were maintained at 37°C with 5% CO_2 in a serum-free culture medium consisting of Neurobasal medium (Invitrogen, 21103-049) supplemented with 2.5 mM L-glutamine (Nacalai Tesque, 16919-55), 2.5% B-27 (Invitrogen, 0050129SA), and 0.01% penicillin/streptomycin. The cultured cells were used for experiments at 5–7 days in vitro.

Immunocytochemistry. Cultures were washed once in PBS and fixed with 4% paraformaldehyde for 20 min. After rinsing with PBS, the cells were permeabilized with 0.2% Triton X-100 in PBS with 2% normal goat serum and 2% bovine serum albumin for 1 h at 4°C. Immunocytochemical staining was performed using antibodies against microtubule-associated protein 2 (1:500; Millipore, AB5622), tau1 (1:100; Millipore, MAB3420) and lamp-1 (1:100; Stressgen, VAM-EN001), followed by incubation with Alexa 488- and Alexa 546-conjugated secondary antibodies (1:1,000; Molecular Probes). The stained cells were viewed using a fluorescence microscope (Nikon) or a confocal laser-scanning microscope (Fluoview; Olympus).

Live-cell imaging. For the time-lapse imaging experiments, the cover slips were transferred to an experimental chamber, washed three times, and resuspended in artificial cerebrospinal fluid solution (110 mM NaCl, 5 mM KCl, 1 mM $CaCl_2$, 10 mM glucose and 20 mM HEPES, pH 7.3 with KOH). Cells were maintained at 35°C by heating the experimental chamber (Medical systems corp, TC-202). The fluorescence of GFP-LC3 was visualized under an inverted microscope (Olympus, IX-70) and a 60x objective (NA 1.42; Olympus) using standard filter sets and a mercury lamp. Sequential images were acquired with a cooled CCD camera (Hamamatsu Photonics, ORCA-ER) equipped with a motorized filter wheel (Sutter Instrument, Lambda 10-2) controlled by the TI Work Bench software (written by T. Inoue). Images were taken every 10 s for 5 min. The distance each GFP-LC3 dot moved between two frames was measured using TI Work Bench. The mean number of autophagosomes was calculated by counting the number of GFP-LC3 dots in 30 randomly set 10-μm-long axon regions that were located farther than 200 μm from the microexplant core.

Western blot analysis. Cultured granule cells were solubilized in TNE buffer (50 mM NaF, 1% NP-40, 20 mM EDTA, 1 μM pepstatins, 2 μg/ml leupeptin, 10 μg/ml aprotinin, 0.1% SDS, 50 mM Tris-HCl, pH 8.0) for 1 h at 4°C. Soluble and insoluble fractions were separated by centrifugation at 11,500 *xg* for 20 min. Both fractions were incubated in SDS-PAGE sample buffer for 5 min at 95°C. After centrifugation, the supernatant was loaded onto SDS-polyacrylamide gels. The proteins were transferred to polyvinylidene difluoride membranes (Immobilon-P, Millipore), allowed to react with antibodies against LC3 (1:500) (Nanotool, 0231-100), p62/SQSTM1 (1:100) (Progen, GP62-C) or actin (1:500) (Sigma, A4700). Proteins were visualized using the chemiluminescence detection system ECL Plus (Amersham Pharmacia).

Chemicals. EHNA (erythro-9-[3-(2-hydroxynonyl)] adenine) (Sigma, E114), NMDA (*N*-methyl-D-aspartate) (Sigma, M3262), glycine (Sigma, 15527), APV (D-2-Amino-5-phosphono-valeric acid) (Sigma, A5282), and bafilomycin A1 (Wako, 023-11641) were used in this study.

Data analysis. The results are presented as the means ± SEM, and a p value < 0.05 was considered significant. The data were evaluated using an unpaired Student's t test. Nonparametric data were evaluated using the Mann-Whitney *U* test using Statview software (SAS Institute Inc.,).

Acknowledgements

We thank Sakae Narumi for technical assistance. This work was supported by a Grant-in-Aid from the Ministry of Education, Culture, Sports, Science and Technology of Japan (M.Y.), the Takeda Science Foundation (M.Y.), and the Japan Society for the Promotion of Science (J.N.).

Note

Supplementary materials can be found at:
www.landesbioscience.com/supplement/KatsumataAUTO6-3-Sup.pdf
www.landesbioscience.com/supplement/KatsumataAUTO6-3-Sup.mpeg

References

1. Reggiori F, Klionsky DJ. Autophagy in the eukaryotic cell. Eukaryot Cell 2002; 1:11-21.
2. Klionsky DJ, Cregg JM, Dunn WA Jr, Emr SD, Sakai Y, Sandoval IV, et al. A unified nomenclature for yeast autophagy-related genes. Dev Cell 2003; 5:539-45.
3. Kuma A, Hatano M, Matsui M, Yamamoto A, Nakaya H, Yoshimori T, et al. The role of autophagy during the early neonatal starvation period. Nature 2004; 432:1032-6.
4. Komatsu M, Waguri S, Ueno T, Iwata J, Murata S, Tanida I, et al. Impairment of starvation-induced and constitutive autophagy in Atg7-deficient mice. J Cell Biol 2005; 169:425-34.
5. Hara T, Nakamura K, Matsui M, Yamamoto A, Nakahara Y, Suzuki-Migishima R, et al. Suppression of basal autophagy in neural cells causes neurodegenerative disease in mice. Nature 2006; 441:885-9.
6. Komatsu M, Waguri S, Chiba T, Murata S, Iwata J, Tanida I, et al. Loss of autophagy in the central nervous system causes neurodegeneration in mice. Nature 2006; 441:880-4.
7. Komatsu M, Wang QJ, Holstein GR, Friedrich VL Jr, Iwata J, Kominami E, et al. Essential role for autophagy protein Atg7 in the maintenance of axonal homeostasis and the prevention of axonal degeneration. Proc Natl Acad Sci USA 2007; 104:14489-94.
8. Nishiyama J, Miura E, Mizushima N, Watanabe M, Yuzaki M. Aberrant membranes and double-membrane structures accumulate in the axons of Atg5-null Purkinje cells before neuronal death. Autophagy 2007; 3:591-6.
9. Kroemer G, Levine B. Autophagic cell death: the story of a misnomer. Nat Rev Mol Cell Biol 2008; 9:1004-10.
10. Cuervo AM. Autophagy: in sickness and in health. Trends Cell Biol 2004; 14:70-7.
11. Rubinsztein DC, DiFiglia M, Heintz N, Nixon RA, Qin ZH, Ravikumar B, et al. Autophagy and its possible roles in nervous system diseases, damage and repair. Autophagy 2005; 1:11-22.
12. Boland B, Kumar A, Lee S, Platt FM, Wegiel J, Yu WH, et al. Autophagy induction and autophagosome clearance in neurons: relationship to autophagic pathology in Alzheimer's disease. J Neurosci 2008; 28:6926-37.
13. Ravikumar B, Vacher C, Berger Z, Davies JE, Luo S, Oroz LG, et al. Inhibition of mTOR induces autophagy and reduces toxicity of polyglutamine expansions in fly and mouse models of Huntington disease. Nat Genet 2004; 36:585-95.
14. Cai ZL, Shi JJ, Yang YP, Cao BY, Wang F, Huang JZ, et al. MPP+ impairs autophagic clearance of alpha-synuclein by impairing the activity of dynein. Neuroreport 2009; 20:569-73.

15. Borsello T, Croquelois K, Hornung JP, Clarke PG. N-methyl-d-aspartate-triggered neuronal death in organotypic hippocampal cultures is endocytic, autophagic and mediated by the c-Jun N-terminal kinase pathway. Eur J Neurosci 2003; 18:473-85.
16. Tarabal O, Caldero J, Casas C, Oppenheim RW, Esquerda JE. Protein retention in the endoplasmic reticulum, blockade of programmed cell death and autophagy selectively occur in spinal cord motoneurons after glutamate receptor-mediated injury. Mol Cell Neurosci 2005; 29:283-98.
17. Mizushima N, Yamamoto A, Matsui M, Yoshimori T, Ohsumi Y. In vivo analysis of autophagy in response to nutrient starvation using transgenic mice expressing a fluorescent autophagosome marker. Mol Biol Cell 2004; 15:1101-11.
18. Yang Y, Fukui K, Koike T, Zheng X. Induction of autophagy in neurite degeneration of mouse superior cervical ganglion neurons. Eur J Neurosci 2007; 26:2979-88.
19. Yue Z. Regulation of neuronal autophagy in axon: implication of autophagy in axonal function and dysfunction/degeneration. Autophagy 2007; 3:139-41.
20. Kuma A, Matsui M, Mizushima N. LC3, an autophagosome marker, can be incorporated into protein aggregates independent of autophagy: caution in the interpretation of LC3 localization. Autophagy 2007; 3:323-8.
21. Yamasaki T, Kawaji K, Ono K, Bito H, Hirano T, Osumi N, et al. Pax6 regulates granule cell polarization during parallel fiber formation in the developing cerebellum. Development 2001; 128:3133-44.
22. Nakatsuji N, Nagata I. Paradoxical perpendicular contact guidance displayed by mouse cerebellar granule cell neurons in vitro. Development 1989; 106:441-7.
23. Kawaji K, Umeshima H, Eiraku M, Hirano T, Kengaku M. Dual phases of migration of cerebellar granule cells guided by axonal and dendritic leading processes. Mol Cell Neurosci 2004; 25:228-40.
24. Ekstrom P, Kanje M. Inhibition of fast axonal transport by erythro-9-[3-(2-hydroxynonyl)]adenine. J Neurochem 1984; 43:1342-5.
25. Forman DS, Brown KJ, Promersberger ME. Selective inhibition of retrograde axonal transport by erythro-9-[3-(2-hydroxynonyl)]adenine. Brain Res 1983; 272:194-7.
26. Koike M, Shibata M, Waguri S, Yoshimura K, Tanida I, Kominami E, et al. Participation of autophagy in storage of lysosomes in neurons from mouse models of neuronal ceroid-lipofuscinoses (Batten disease). Am J Pathol 2005; 167:1713-28.
27. Klionsky DJ, Abeliovich H, Agostinis P, Agrawal DK, Aliev G, Askew DS, et al. Guidelines for the use and interpretation of assays for monitoring autophagy in higher eukaryotes. Autophagy 2008; 4:151-75.
28. Yamamoto A, Tagawa Y, Yoshimori T, Moriyama Y, Masaki R, Tashiro Y. Bafilomycin A1 prevents maturation of autophagic vacuoles by inhibiting fusion between autophagosomes and lysosomes in rat hepatoma cell line, H-4-II-E cells. Cell Struct Funct 1998; 23:33-42.
29. Mizushima N, Yoshimori T. How to interpret LC3 immunoblotting. Autophagy 2007; 3:542-5.
30. Rubinsztein DC, Cuervo AM, Ravikumar B, Sarkar S, Korolchuk V, Kaushik S, et al. In search of an "autophagomometer". Autophagy 2009; 5:585-9.
31. Bjorkoy G, Lamark T, Brech A, Outzen H, Perander M, Overvatn A, et al. p62/SQSTM1 forms protein aggregates degraded by autophagy and has a protective effect on huntingtin-induced cell death. J Cell Biol 2005; 171:603-14.
32. Yue Z, Holstein GR, Chait BT, Wang QJ. Using genetic mouse models to study the biology and pathology of autophagy in the central nervous system. Methods Enzymol 2009; 453:159-80.
33. Selimi F, Lohof AM, Heitz S, Lalouette A, Jarvis CI, Bailly Y, et al. Lurcher GRID2-induced death and depolarization can be dissociated in cerebellar Purkinje cells. Neuron 2003; 37:813-9.
34. Kimura S, Noda T, Yoshimori T. Dynein-dependent movement of autophagosomes mediates efficient encounters with lysosomes. Cell Struct Funct 2008; 33:109-22.
35. Jahreiss L, Menzies FM, Rubinsztein DC. The itinerary of autophagosomes: from peripheral formation to kiss-and-run fusion with lysosomes. Traffic 2008; 9:574-87.
36. Shacka JJ, Lu J, Xie ZL, Uchiyama Y, Roth KA, Zhang J. Kainic acid induces early and transient autophagic stress in mouse hippocampus. Neurosci Lett 2007; 414:57-60.
37. Zuo J, De Jager PL, Takahashi KA, Jiang W, Linden DJ, Heintz N. Neurodegeneration in Lurcher mice caused by mutation in delta2 glutamate receptor gene. Nature 1997; 388:769-73.
38. Kohda K, Wang Y, Yuzaki M. Mutation of a glutamate receptor motif reveals its role in gating and delta2 receptor channel properties. Nat Neurosci 2000; 3:315-22.
39. Wang QJ, Ding Y, Kohtz DS, Mizushima N, Cristea IM, Rout MP, et al. Induction of autophagy in axonal dystrophy and degeneration. J Neurosci 2006; 26:8057-68.
40. Nishiyama J, Matsuda K, Kakegawa W, Yamada N, Motohashi J, Mizushima N, et al. Reevaluation of neurodegeneration in lurcher mice: constitutive ion fluxes cause cell death with, not by, autophagy. J Neurosci in press.
41. Lakadamyali M, Rust MJ, Babcock HP, Zhuang X. Visualizing infection of individual influenza viruses. Proc Natl Acad Sci USA 2003; 100:9280-5.
42. Bannai H, Inoue T, Nakayama T, Hattori M, Mikoshiba K. Kinesin dependent, rapid, bi-directional transport of ER sub-compartment in dendrites of hippocampal neurons. J Cell Sci 2004; 117:163-75.
43. Ravikumar B, Acevedo-Arozena A, Imarisio S, Berger Z, Vacher C, O'Kane CJ, et al. Dynein mutations impair autophagic clearance of aggregate-prone proteins. Nat Genet 2005; 37:771-6.
44. Hanawa H, Kelly PF, Nathwani AC, Persons DA, Vandergriff JA, Hargrove P, et al. Comparison of various envelope proteins for their ability to pseudotype lentiviral vectors and transduce primitive hematopoietic cells from human blood. Mol Ther 2002; 5:242-51.
45. Torashima T, Okoyama S, Nishizaki T, Hirai H. In vivo transduction of murine cerebellar Purkinje cells by HIV-derived lentiviral vectors. Brain Res 2006; 1082:11-22.
46. Forrest D, Yuzaki M, Soares HD, Ng L, Luk DC, Sheng M, et al. Targeted disruption of NMDA receptor 1 gene abolishes NMDA response and results in neonatal death. Neuron 1994; 13:325-38.
47. Kurschner C, Yuzaki M. Neuronal interleukin-16 (NIL-16): a dual function PDZ domain protein. J Neurosci 1999; 19:7770-80.

Regional Spinal Cord Cooling Using a Countercurrent Closed-Lumen Epidural Catheter

Hideyuki Shimizu, MD, PhD, Atsuo Mori, MD, PhD, Tatsuya Yamada, MD, PhD, Akiko Ishikawa, MD, Hideyuki Okano, MD, PhD, Junzo Takeda, MD, PhD, and Ryohei Yozu, MD, PhD

Departments of Cardiovascular Surgery, Anesthesiology, and Physiology, Keio University, Shinjuku-ku, Tokyo, Japan

We developed a method of regional spinal cord cooling by using an epidural catheter containing cold saline in its isolated counter-current lumen. We describe the clinical application of this innovative procedure to the prevention of paraplegia during surgery for thoracic and thoracoabdominal aortic aneurysms.

(Ann Thorac Surg 2010;89:1312–3)

Paraplegia associated with surgery for thoracic and thoracoabdominal aortic aneurysm remains a devastating complication. We previously demonstrated the ability of regional spinal cord cooling using a custom-designed epidural catheter to prevent ischemic spinal cord injury in experimental studies using pigs [1, 2]. We applied this novel system in a clinical setting.

Technique

Patients

Six patients (4 men, 2 women; aged 57 to 80 years) with aneurysms of the descending thoracic (5 patients) or thoracoabdominal (1 patient) aorta underwent elective surgery using our novel cooling method between September 2008 and January 2009. The cause of aortic disease was atherosclerotic aneurysm (n = 3), aortic dissection (n = 2), and pseudoaneurysm after infection (n = 1). Four of the 6 patients had prior operations on the abdominal aorta (n = 2), the transverse aorta (n = 1), and both (n = 1). The Institutional Review Board of Keio University Hospital approved the study, and written, informed consent was obtained from each patient to participate in all procedures associated with the study.

Continuous Cord Cooling System Using a Custom-Designed Epidural Catheter

A custom-designed polyurethane epidural catheter (Unitika, Tokyo, Japan) (Fig 1), an external circuit tube, and a pump with a hollow fiber heat exchanger (Senko-Ika Co, Ltd, Tokyo, Japan) comprised a circuit (Fig 2). The catheter (16-gauge outer diameter; length, 30 cm) has two ends that form the inlet and outlet of a single U-shaped closed lumen inside it. The direction of the flow of saline infused from the inlet reverses at the tip of the catheter and flows out of the outlet. The temperature of the saline is reduced to 12°C to 13°C by a cooling unit, infused into the inlet of the countercurrent catheter and then circulated by an external roller pump at an approximate flow rate of 60 mL/min.

Percutaneous Installation of Cooling Catheter

The catheter was positioned percutaneously on the day before surgery. Patients were placed in the prone position. A local anesthetic was applied and then the skin on the back was punctured with a special epidural Touhy-type needle with a thin polyurethane outer-sheath (Unisis-Unitika, Tokyo, Japan) through the paramedian approach at level 1 to 2 of the lumbar spine. The needle was advanced until the tip reached the epidural space and then removed without moving the outer sheath. The cooling catheter was introduced into the epidural space through the outer sheath, and was advanced in the direction of the head as far as it could contact the segment of the spinal cord that would be under ischemic stress during aortic cross clamping. Fluoroscopic guidance confirmed the proper placement, after which the outer sheath was peeled off. The catheter was affixed to the skin and left in situ until surgery.

Surgical Procedure, External Corporeal Bypass, and Epidural Cooling Protocol

Surgery proceeded with patients in the right-sided lateral position. A left thoracotomy was performed through an appropriate intercostal space. The skin incision was extended toward the umbilicus, and the diaphragm was divided in 1 patient with a thoracoabdominal aortic aneurysm. Heparin sulfate was injected intravenously, and then a femoro-femoral bypass with a centrifugal pump and a membrane oxygenator was established for distal perfusion during aortic cross clamping. We did not actively cool the blood with an external heat-exchanger, although the rectal temperature spontaneously dropped to 33.6°C to 36.2°C. The aorta was cross clamped using the serial shift technique in 2 patients and was replaced with prosthetic grafts. The intercostal arteries were reconstructed in a beveled fashion in 4 patients, and the celiac and superior mesenteric arteries were reconstructed using a branched graft in 1. Regional spinal cord cooling was started 30 minutes beforehand, continued during aortic cross clamping, and terminated 30 minutes after unclamping. None of the patients underwent cerebrospinal fluid drainage. Motor-evoked potentials (MEPs) were monitored in all patients.

Accepted for publication June 9, 2009.

Address correspondence to Dr Shimizu, Department of Cardiovascular Surgery, 35 Shinanomachi, Shinjuku-ku, Tokyo, 160-8582, Japan; e-mail: hideyuki@sc.itc.keio.ac.jp.

Published by Elsevier Inc

0003-4975/10/$36.00
doi:10.1016/j.athoracsur.2009.06.045

Results

The mean durations of aortic cross clamping and external corporeal bypass were 52.0 ± 18.7 and 65.3 ± 19.5 minutes, respectively. Motor-evoked potentials did not disappear during or after aortic cross clamping in any of the patients, and none of them died in the hospital. All patients recovered full use of their lower limbs with no paraplegia or paraparesis on the day of surgery. Complications, including coagulopathy and cardiac events, did not arise.

Comment

Paraplegia remains the most serious complication associated with thoracic and thoracoabdominal aortic aneurysm. Hypothermia is one of the most reliable methods of protecting the spinal cord from ischemia, but systemic hypothermia confers several risks, including coagulopathy, arrhythmia, and lung dysfunction. Cambria and coworkers [3] described favorable clinical results of local cooling by infusing iced saline into the epidural space during aortic cross clamping. However, it might cause a detrimental increase in cerebrospinal fluid pressure. To avoid such adverse effects, we developed an alternative technique for epidural cooling using a custom-designed countercurrent catheter. We demonstrated in pigs that a cooling catheter containing saline at a temperature of 4°C circulating at a flow rate of 45 mL/min could cool the spinal cord by 9.7°C without elevating cerebrospinal fluid pressure. The spinal cord was protected from 45 minutes of ischemia, induced by aortic cross clamping without distal perfusion [1, 2]. Based on these results as well as the outlet temperature of the circulating saline, we determined the cooling conditions for clinical applications.

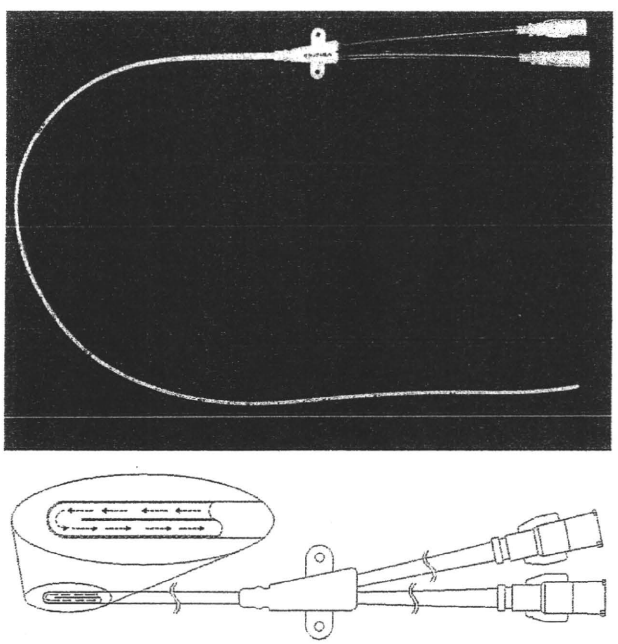

Fig 1. Epidural cooling catheter. Cold saline circulates in closed lumen of catheter, turning back at tip without leakage.

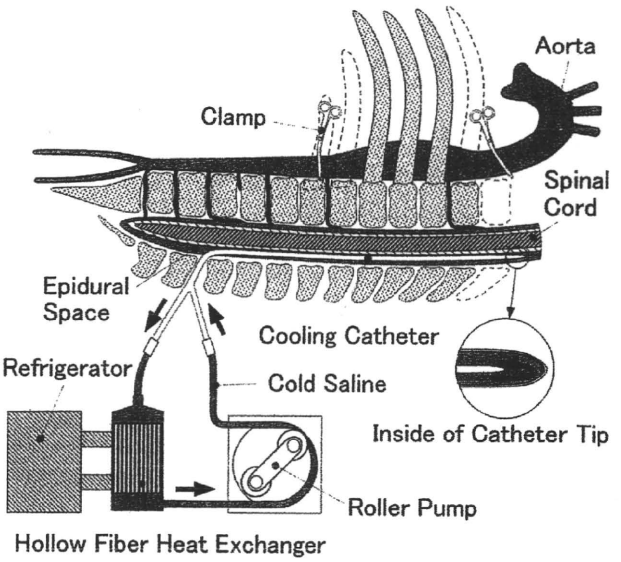

Fig 2. Schematic illustration of continuous cord cooling system. Closed loop circuit comprises epidural cooling catheter, circulating pump, and hollow-fiber cooling unit.

We did not measure cerebrospinal fluid temperature and pressure to avoid the complexity of installing another catheter. However, such measurements might be helpful to rigorously adjust cooling conditions for each individual. The combination of epidural cooling and cerebrospinal fluid drainage might be a promising strategy.

We also developed a Touhy-style epidural needle with an outer sheath that can be peeled off. This modification allowed installation of the catheter into the epidural space without laminectomy, similar to epidural pacing lead placement against phantom pain control.

Although our patient cohort was small, the clinical application of regional spinal cord cooling using a custom-designed countercurrent epidural catheter proved successful as an additional protection against paraplegia. Further clinical trials are warranted to confirm that this technique protects against paraplegia during surgery for thoracic and thoracoabdominal aortic aneurysms.

This study was supported by a Grant-in-Aid for Scientific Research (C) of the Ministry of Education, Culture, Sports, Science, and Technology. We express special thanks to Nobuyuki Kabei, PhD for excellent technical assistance.

References

1. Mori A, Ueda T, Hachiya T, et al. An epidural cooling catheter protects the spinal cord against ischemic injury in pigs. Ann Thorac Surg 2005;80:1829–34.
2. Yoshitake A, Mori A, Shimizu H, et al. Use of an epidural cooling catheter with a closed countercurrent lumen to protect against ischemic spinal cord injury in pigs. J Thorac Cardiovasc Surg 2007;134:1220–6.
3. Cambria RP, Clouse WD, Davison JK, Dunn PF, Corey M, Dorer D. Thoracoabdominal aneurysm repair: results with 317 operations performed over a 15-year interval. Ann Surg 2002;236:471–9.

短　報

気管切開が施行不能であった頸部海綿状血管腫の1症例

壽原　朋宏*　森山　　潔**　細川　幸希*　藍　　公明*　武田　純三*

キーワード：CICV，頸部海綿状血管腫，レミフェンタニル

血管腫は全体の約65%が頭頸部に発生し，大部分は鼻腔副鼻腔領域にできる[1]。気道および気道周辺に発生した血管腫に対し外科的処置が必要な場合，気道確保に際して綿密な計画が必要となる。今回，下咽頭・喉頭・気管周囲から縦隔まで連続する広範な病変を有し，気管切開が施行不能であった頸部海綿状血管腫の1症例を経験したので報告する。

1. 症　　例

48歳，女性，身長152 cm，体重45 kg

幼少時より嗄声を認め，38歳時に近医で下咽頭血管腫を指摘された。48歳となり呼吸困難が出現し，下咽頭血管腫に対する手術目的で当院耳鼻科を受診した。初診時喉頭ファイバーを施行したところ，左被裂部に拇指頭大の有茎性腫瘤を認めた。腫瘤は発声時に喉頭腔への嵌頓を認め，呼吸困難の原因と考えられた。頸部コンピュータ断層撮影（computed tomography：CT）では喉頭上部より左声門に膨隆する長径2.5 cmの腫瘤性病変を認めた（図1）。病変は前頸部より後頸部・縦隔まで連続し，甲状腺両葉にも浸潤を認めた。多数の静脈結石を認め，高血流の静脈性血管奇形を伴う頸部海綿状血管腫と診断された。前頸部は舌骨の下方1 cmより尾側に病変が連続しており（図2），病変を避けての気管切開は困難が予想されたが，全身麻酔下気管切開（第1気管輪レベル）および咽頭側切開下咽頭腫瘍摘出術が予定された。

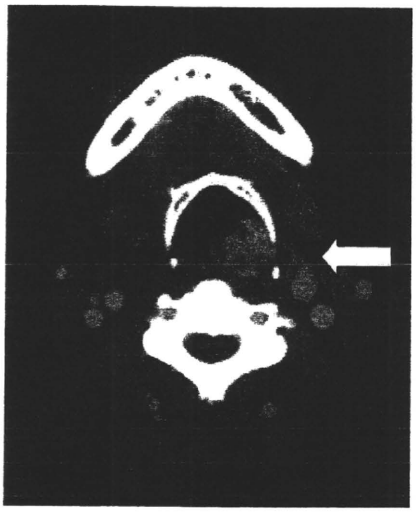

図1　喉頭上部より左声門に膨隆する長径2.5 cmの腫瘤性病変（矢印）を認める。

麻酔導入に際しては，下咽頭の有茎性血管腫による気道閉塞，換気困難・気管挿管困難（cannot intubate, cannot ventilate：CICV）の可能性が考えられた。また，術前検査より輪状甲状間膜切開および気管切開も困難が予想されたため，意識下での経口気管支ファイバー挿管を予定した。手術室入室後，硫酸アトロピン0.5 mgを静注，8%リドカイン0.9 mlを口腔内に噴霧し，酸素マスクで5分間の脱窒素化を行った。レミフェンタニルを0.1 $\mu g \cdot kg^{-1} \cdot min^{-1}$で持続投与開始し，患者に深呼吸を促しながら0.2 $\mu g \cdot kg^{-1} \cdot min^{-1}$まで漸増した。経鼻カニューレで酸素3 $l \cdot min^{-1}$を投与しながら口腔内に経口エアウェイ挿入し，口腔内分泌物吸引後に仰臥位で外径5.0 mmの気管支ファ

* 慶應義塾大学医学部麻酔学教室
** 杏林大学医学部麻酔科学教室
2009年3月5日受領：2009年6月30日掲載決定

図 2　前頸部は舌骨の下方 1 cm より尾側に血管腫病変（矢印）が連続している。

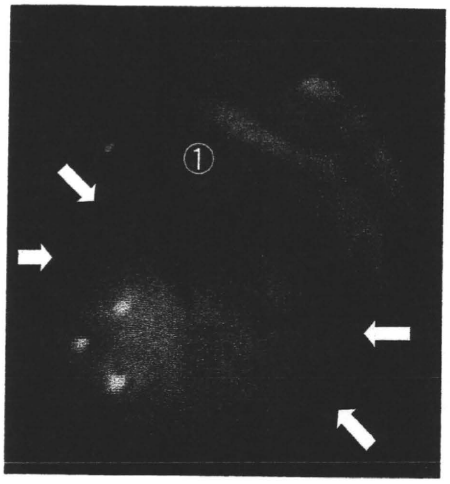

図 3　仰臥位でのファイバー挿管試行時血管腫（矢印）で閉塞され声門部は視認不能であった。①：喉頭蓋

イバーを挿入したが，血管腫で閉塞され声門部は視認不能であった（図 3）。患者を半坐位として再施行し，助手が下顎を挙上したところわずかに声門部が視認できた。4%リドカイン 5 ml を噴霧しつつ気管支ファイバーを気管分岐部まで進め，気管支ファイバーをガイドとして内径 6.5 mm のスタンダードチューブを気管挿管した。気管挿管後の麻酔は酸素 $2\,l \cdot \mathrm{min}^{-1}$，空気 $4\,l \cdot \mathrm{min}^{-1}$，セボフルラン 1.5-2%およびレミフェンタニル 0.2-0.25 $\mu\mathrm{g} \cdot \mathrm{kg}^{-1} \cdot \mathrm{min}^{-1}$の持続投与で維持した。

手術はまず全身麻酔下で気管切開を試みたが，気管前壁の血管腫より多量の出血があり視野確保に難渋した。エフェドリン総量 40 mg およびフェニレフリン総量 50 μg の間歇的静注およびヒドロキシエチルデンプン注射液 1,500 ml の補液により血圧を維持していたが，手術開始 3 時間後には出血が 1,000 g を超え，収縮期血圧が 70 mmHg，ヘモグロビン（hemoglobin：Hb）が $7.4\,\mathrm{g} \cdot \mathrm{dl}^{-1}$まで低下したため赤血球濃厚液の輸血を開始した。その後も出血は続き，手術進行不可能と考えられたため気管切開せずに止血して手術終了となった。手術時間は 4 時間 10 分，術中出血は 1,880 g，術中輸血は赤血球濃厚液 4 単位であった。

患者は気管挿管したまま集中治療室（intensive care unit：ICU）に帰室し，鎮静下に人工呼吸管理を継続した。ICU 帰室後も出血は持続し，赤血球濃厚液計 8 単位を輸血した。ICU で人工呼吸管理を継続した後，第 7 病日に左咽頭側切開アプローチで下咽頭腫瘍切除術を施行した。甲状軟骨後面より咽頭腔に入り，血管腫の茎を確認して切除した。手術時間は 2 時間 42 分，術中出血は 5 g であった。術後喉頭ファイバーによる観察と頻繁にリークテストを行い気道の開通を確認し，喉頭浮腫予防にデキサメタゾン 8 mg を投与した後，第 9 病日に抜管した。抜管後気道狭窄音を認めたが，残存する前頸部血管腫のために気管切開および輪状甲状間膜切開は不可能と考えられたため，非侵襲的陽圧換気法（non-invasive positive pressure ventilation：NPPV）を導入した。NPPV 導入後気道狭窄音は減弱し，喉頭浮腫が改善したため第 13 病日で NPPV を離脱した。NPPV 離脱後，経鼻カニューレでの酸素 $3\,l \cdot \mathrm{min}^{-1}$投与下で Pa_{O_2} 180 mmHg と経過良好であったため，第 14 病日に一般病床へ転床となった。

2. 考　察

本症例は下咽頭に有茎性の血管腫を認め，術前から CICV が予測された。また喉頭・気管腹側には舌骨の下方 1 cm より尾側に病変が連続しているため，気管切開・輪状甲状間膜切開などの侵襲的気道確保も困難と考えられた。CICV が予測される症例では，米国麻酔科学会（American Society

of Anesthesiologists：ASA）difficult airway algorithm[2]で意識下挿管が推奨されている。本症例では，麻酔導入時の気道確保方法として自発呼吸温存下での意識下ファイバー挿管を選択したが，その主な理由には，① 意識下であれば全身麻酔導入後よりも上気道の開通が維持でき下咽頭の視野が良好である，② 直達喉頭鏡を使用した気管挿管と比べてファイバー挿管のほうが腫瘍への接触が少ないことから出血が少なく気道の観察も行いやすい，という2点が挙げられる。ファイバー操作時およびガイド下にチューブを進める際に下咽頭血管腫を傷つけて出血させてしまう可能性はあったが，無理をせずに抵抗があればチューブを回転させながらゆっくりと進めることでリスクは最小限になると考えた。

意識下ファイバー挿管に際してレミフェンタニル持続投与による鎮痛は患者の苦痛除去と喉頭の防御反射抑制に有用であると報告されており[3]，リドカインの鼻腔粘膜局所噴霧とレミフェンタニル持続投与の併用で意識下ファイバー挿管時に安定した呼吸・循環動態が得られたことが報告されている[4]。意識下ファイバー挿管に併用される上喉頭神経ブロックや経喉頭ブロックは，前頸部血管腫からの出血や薬液の血管内投与の危険性が高く本症例では禁忌と考えられた。また，本症例ではリドカイン噴霧とレミフェンタニル持続静注を併用し，気管支ファイバーの操作中も適度な鎮痛・鎮静が維持できた。仰臥位で声門部視認不可能であった場合は，患者に深呼吸を促すとともに下顎を挙上することで下咽頭のスペースが広がり視野が改善することが報告されている[5]。

ASA difficult airway algorithm[2]では，意識下挿管で気道確保が不成功に終わった場合，① 他のオプションを考慮する，② 侵襲的気道確保，③ 手術中止，の3つが選択肢として挙げられている。① 他のオプションにはラリンジアルマスク（laryngeal mask airway：LMA）による気道確保，局所麻酔下での手術が挙げられる。本症例ではLMAは手術操作の妨げになるだけでなく，挿入時に血管腫を傷つけて出血し，挿入できても腫瘍が声門部を覆っていれば換気不可能になることも考えられた。局所麻酔下での手術は気道が術野であり不可能であった。また代替の挿管手段であるintubating LMA，光源付きスタイレット，エラスティックブジー，エアウェイスコープなどは，ファイバーによる声門部視認が困難な本症例では有効とはいい難い。② 侵襲的気道確保については，コントロール不可能な大量出血の危険性を考えると躊躇せざるをえない。よって本症例で挿管不可能と判断した場合には，③ 手術中止の選択が残される。その際にはレミフェンタニルの投与を中止すればすみやかな全覚醒が期待できる。なお，レミフェンタニル投与中に筋硬直や自発呼吸停止が起こった場合にも，ナロキソン静注により対処可能であると考えた。気管支ファイバーとの接触により下咽頭血管腫から出血させて挿管不可能となった場合には，前頸部出血のリスクがあっても緊急で輪状甲状間膜切開を施行し，ただちに経皮的心肺補助装置（PCPS）を導入することも念頭におく必要があった。

換気・挿管・気管切開困難が予測された頸部海綿状血管腫の症例を経験した。本症例の麻酔導入に際して，リドカイン噴霧とレミフェンタニル持続静注を併用した意識下ファイバー挿管により安全な気道確保を実施できた。

引用文献

1) 甲能直幸. 血管腫. 犬山征夫編. 頭頸部腫瘍. CLIENT 21 No. 17. 第1版. 東京：中山書店；2000. p.282-9.
2) American Society of Anesthesiologists. Practice Guidelines for Management of the Difficult Airway. Anesthesiology 2003；98：1269-77.
3) Puchner W, Egger P, Pühringer F, Löckinger A, Obwegeser J, Gombotz H. Evaluation of remifentanil as single drug for awake fiberoptic intubation. Acta Anaesthesiol Scand 2002；46：350-4.
4) Mingo OH, Ashpole KJ, Irving CJ, Rucklidge MW. Remifentanil sedation for awake fiberoptic intubation with limited application of local anaesthetic in patients for elective head and neck surgery. Anaesthesia 2008；63：1065-9.
5) 佐登宣仁, 中澤　直, 中筋　勲, 新宮　興. ファイバー挿管に下顎挙上が有用であった喉頭蓋嚢胞

の1症例. 麻酔 2002；51：910-2.

ABSTRACT

Airway Management in a Patient with Cavernous Hemangioma of the Hypopharynx and Larynx

Tomohiro SUHARA, Kiyoshi MORIYAMA*,
Yuki HOSOKAWA, Kimiaki AI,
Junzo TAKEDA

Department of Anesthesiology, School of Medicine, Keio University, Tokyo 160-8582
**Department of Anesthesiology, Kyorin University Faculty of Medicine, Tokyo 181-8611*

A 48-year-old woman was diagnosed with cavernous hemangioma of hypopharynx and larynx, which extended to the trachea and mediastinum. She was scheduled for tracheostomy and open surgical excision of hypopharynx hemangioma under general anesthesia. On induction of anesthesia, we planned awake fiberoptic intubation according to the difficult airway algorithm of the American Society of Anesthesiologists. Under continuous infusion of remifentanil at 0.1-0.2 $\mu g \cdot kg^{-1} \cdot min^{-1}$, the patient became sedated while spontaneously breathing, and her pain and laryngeal reflexes were reduced. Although tracheal intubation was successfully accomplished without injuring the hypopharynx hemangioma, tracheostomy was difficult because of bleeding from the surgical site. After 3hr of surgery with 1,880 g of blood loss, the surgeons quitted tracheostomy and the patient was transferred to the intensive care unit. Her airway was managed with endotracheal tube for 7 days, and open surgical excision of hypopharynx hemangioma was performed on day 7. The patient was successfully extubated on day 9 with the support of non-invansive positive pressure ventilation. Awake fiberoptic intubation under remifentanil infusion is safe and useful approach for patients with airway hemangioma.

key words：airway hemangioma, awake fiberoptic intubation, remifentanil

35

Laudanosine has No Effects on Respiratory Activity but Induces Non-Respiratory Excitement Activity in Isolated Brainstem-Spinal Cord Preparation of Neonatal Rats

Shigeki Sakuraba[1], Yuki Hosokawa[1], Yuki Kaku[2], Junzo Takeda[1], and Shun-ichi Kuwana[2]

[1] Department of Anesthesiology, Keio University, Tokyo, Japan, shigekisakuraba@gmail.com
[2] Department of Physiology, Uekusa University, Chiba, Japan

Abstract Laudanosine, a degradation of neuomuscular blocking agent atracurium, crosses the blood-brain barrier and is indicted to trigger seizures at high concentration. In *Xenopus Oocytes* expressing nicotinic acetylcholine receptors (nAChRs), laudanosine has activating and inhibiting effects on nAChRs depending on its concentration. nAChRs is related to respiratory activities and thus, in the present study, we analyzed effects of laudanosine on central respiratory activities using isolated brainstem-spinal cord preparation of neonatal rats. The rhythmic inspiratory burst activity of the C4 spinal ventral root was recorded using a glass suction electrode as an index of respiratory rate. After superfusion with mock cerebrospinal fluid (CSF), the preparation was superfused with mock CSF containing laudanosine 1, 10 or 100 μM for 60 minutes. Laudanosine 1, 10 and 100 μM (n = 10 in each) did not induce any effects on C4 respiratory rate. In all 10 preparations, laudnosine 100 μM induced non-respiratory excitement activities that are possibly same as seizure observed in vivo study.

1 Introduction

Laudanosine is a metabolite of the neuromuscular blocking agent atracurium (Fodale and Santamaria 2002). It crosses the blood-brain barrier and accumulates in the cerebrospinal fluid (CSF) (Eddleston et al. 1989; Tassonyi et al. 2002), although neuromuscular blocking agents do not cross the blood-brain barrier. In the in vivo, laudanosine penetrated into CSF induces excitement (Lanier et al. 1985; Beemer et al. 1989) and seizure (Chapple et al. 1987).

Although laudanosine has no muscle relaxation effects via muscular nicotinic acetylcholine receptor (nAChR), laudanosine induces the dual mode of action on neuronal nAChR; it inhibits α4β2 and α7 neuronal nAChRs expressed in *Xenopus Oocytes* at high concentration, whereas it activates α4β2 neuronal nAChRs at low concentrations (Chiodini et al. 2001). nAChR subunits α4β2 and α7 expressed in ventrolateral medulla modulate respiratory activities (Hatori et al. 2006).

Therefore, we investigated the effects of laudanosine on respiratory activities using isolated brainstem-spinal cord preparation of neonatal rats.

I. Homma et al. (eds.), *New Frontiers in Respiratory Control*,
Advances in Experimental Medicine and Biology 669, DOI 10.1007/978-1-4419-5692-7_35,

2 Methods

This study was approved by the Animal Ethical Committee of Teikyo University Experiments were performed on the brainstem-spinal cord preparation of neonatal Wistar rat (0–4 days old; $n = 30$). The surgical procedure used to make these preparations has been described in detail elsewhere (Sakuraba et al. 2003). Briefly, the rats were deeply anesthetized with diethyl ether, and the brainstem and cervical spinal cord were isolated in a chamber filled with oxygenated mock CSF. Then, the cerebellum and pons were ablated. The isolated preparation was continuously superfused at the rate of 3.5–4.5 mL/min in a 2-ml recording chamber with the ventral side upwards. The preparation was superfused at 26°C with control mock CSF equilibrated with a 95% O_2 and 5% CO_2 (pH = 7.5). The composition of the mock CSF was (in mM) 118 NaCl, 3 KCl, 1.5 $CaCl_2$, 1 $MgCl_2$, 25 $NaHCO_3$, 1.2 NaH_2PO_4, and 30 glucose.

Inspiratory discharges of respiratory motor neurons were monitored by extracellular recording with glass suction electrodes applied to the proximal cut end of C4 ventral roots of spinal nerves, and amplified with a differential AC amplifier (Model 1700, A-M systems, Carlsborg, WA, USA) and integrated (time constant: 100 ms). Axoscope software and Digidata 1200B interface (Axon Instruments, Foster, CA, USA) were used to collect data for off-line analysis.

C4 respiratory rate were calculated from the total number of bursts within a 4-min period before switching the superfusate. After the preparation was superfused with control mock CSF for 20 min and C4 activity reached a steady state, the control superfusate was replaced by a test solution: mock CSF containing laudanosine at 1, 10 and 100 μM (Sigma, St. Louis, MO, USA) for 20 min, followed by a washout period using the mock CSF for 40 min. C4 respiratory rate was counted at 0 min (control), 10 min and 20 min after superfusion with mock CSF containing laudanosine.

Changes in C4 respiratory rate were compared by using one-way analysis variance followed by Dunnet test. $P < 0.05$ was considered significant. Data are expressed as mean ± SD.

3 Results

Laudanosine 1, 10 and 100 μM ($n = 10$ in each) did not induce any effects on C4 respiratory rate (Fig. 1). Laudanosine 100 μM induced non-respiratory excitement activities in all 10 preparations (Fig. 2).

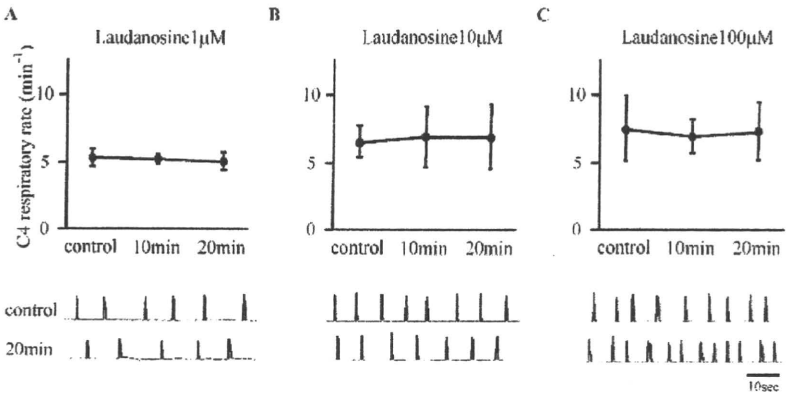

Fig. 1 Effects of laudanosine 1 μM (**A**), 10 μM (**B**) and 100 μM (**C**) on C4 respiratory rate

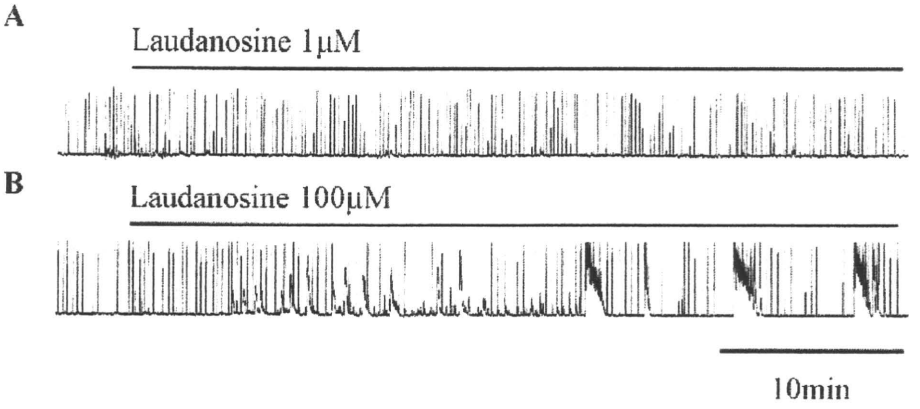

Fig. 2 Representative recording of non-respiratory excitement activities induced by laudanosine 100 μM (**B**). Laudanosine 1μM (**A**) and 10 μM do not induce such activities

4 Discussion

Laudanosine does not induce any changes in respiratory activities. However, it is unclear that it is due to its no effects on central respiratory control or due to its interactive effects on several kinds of receptors because laudanosine is indicated to have effects not only on nAChRs but also on SK channel, opioid receptors and so on. Further pharmacological studies to prevent its potential interactive effects on several receptors are needed.

On the other hand, high concentration of laudanosine induces non-respiratory excitement activities like vecuronium bromide and apamin, SK channel antagonist, reported in the previous studies using the same preparation (Onimaru et al. 1996;

Sakuraba et al. 2003). Therefore, laudanosine may induce non-respiratory excitement activities through neuronal nAChRs or SK channel. Although vecuronium bromide suppresses respiratory activities (Sakuraba et al. 2003), apamin induces no effects on respiratory activities (Onimaru et al. 1996). SK channel expresses on many neurons and inhibits neuron activities by hyperpolarization. Thus, laudanosine-induced non-respiratory excitement activity in the present study is more possibly through SK channel.

In conclusion, laudanosine has no effects on respiratory activities but high concentration of laudanosine induces non-respiratory excitement activities.

Acknowledgments

This study was supported by a Grant-in-Aid for Young Scientist (SS).

References

Beemer, G.H., Bjorksten, A.R., Dawson, P.J., and Crankshaw, D.P. (1989) Production of laudanosine following infusion of atracurium in man and its effects on awakening. Br. J. Anaesh. 63, 76–80.

Chapple, D.J., Mille, A.A., Ward, J.B., and Wheathey, P.L. (1987) Cardiovascular and neurological effects of laudanosine. Studies in mice and rats, and in conscious and anaesthetized dogs. Br. J. Anaesth. 59, 218–225.

Chiodini, F., Charpantier, E., Muller, D., Tassonyi, F., Fuchs-Buder, T., and Bertrand, D. (2001) Blockade and activation of the human neuronal nicotinic acetylcholine receptors by atracurium and laudanosine. Anesthesiology 94, 643–651.

Eddleston, J.M., Harper, N.J., Pollard, B.J., Edwards, D., and Gwonnutt, C.L. (1989) Concentration of atracurium and laudanosine in cerebrospinal fluid and plasma during intracranial surgery. Br. J. Anaesth. 63, 525–530.

Fodale, V., and Santamaria, L.B. (2002) Laudanosine, an atracurium and cisatracurium metabolite. Eur. J. Anaesthesiol. 19, 466–473.

Hatori, E., Sakuraba, S., Kashiwagi, M., Kuribayashi, J., Tsujita, M., Hosokawa, Y., Takeda, J., and Kuwana, S. (2006) Association of nicotinic acetylcholine receptors with central respiratory control in isolated brainstem-spinal cord preparation of neonatal rats. Biol. Res. 39, 321–330.

Lanier, W.L., Milde, J.H., and Michenfelder, J.D. (1985) The cerebral effects of pancuronium and atracurium in halothane-anesthetized dogs. Anesthesiology 63, 1236–1241.

Onimaru, H., Ballanyi, K., and Richter, D.W. (1996) Calcium-dependent responses in neurons of the isolated respiratory network of newborn rats. J. Physiol. 491, 677–695.

Sakuraba, S., Kuwana, S., Ochiai, R., Okada, Y., Kashiwagi, M., Hatori, E., and Takeda, J. (2003) Effects of neuromuscular blocking agents on central respiratory control in the isolated brainstem-spinal cord of neonatal rat. Neurosci. Res. 47, 289–298.

Tassonyi, E., Fathi, M., Hughes, G.J., Chiodini, F., Bertrand, D., Muller, D., and Fuchs-Buder, T. (2002) Cerebrospinal fluid concentrations of atracurium, laudanosine and vecuronium following clinical subarachnoid hemorrhage. Acta. Anaesthesiol. Scand. 46, 1236–1241.

23

Effect of JM-1232(-), a New Sedative on Central Respiratory Activity in Newborn Rats

Junya Kuribayashi[1, 2, 3], Shun-ichi Kuwana[4], Yuki Hosokawa[2], Eiki Hatori[2], and Junzo Takeda[2]

[1] Department of Physiology and Pediatrics, University of Alberta, Edmonton, Canada, junya.kuribayashi@ualberta.ca
[2] Department of Anesthesiology, Keio University School of Medicine, Tokyo, Japan
[3] Department of Anesthesiology, Kitasato Institute Hospital, Tokyo, Japan
[4] Uekusa Gakuen University, Tokyo, Japan

Abstract JM-1232(-), a newly manufactured isoindole derivative, shows sedative effect at a lower concentration compared with propofol. In the present study, we analyzed the response of the central respiratory activity to JM-1232(-). The brainstem-spinal cord of a newborn rat was isolated and was continuously superfused with oxygenated artificial cerebrospinal fluid (ACSF). Rhythmic inspiratory burst activity was recorded from C4 spinal ventral root using a glass suction electrode. We measured C4 burst rate and amplitude of integrated C4 activity. After obtaining a control recording, the preparation was superfused with ACSF containing JM-1232(-) at 10, 100 or 500 μM for 10 min. The application of both 10 and 100 μM JM-1232(-) did not decrease C4 burst rate significantly. However, 500 μM JM-1232(-) reduced C4 burst rate. On the contrary, C4 burst amplitude was not affected by the application of JM-1232(-) for 10 min at any concentrations. In conclusion, JM-1232(-) at a low concentration (but presumably higher than hypnotic dose), did not depress the central respiratory activity, whereas at a high concentration depression was seen.

1 Introduction

JM-1232(-), a newly manufactured isoindole derivative, shows sedative effect at a low concentration and possesses a wide therapeutic index compared with propofol (Kanamitsu et al. 2007). The drug can be used without emulsion because of its water-soluble property (Kanamitsu et al. 2007).

Recently, several studies have showed the effect of JM-1232(-) on nociceptive stimuli (Nishiyama et al. 2008; Chiba et al. 2009) and shivering (Masamune et al. 2009). However, there has been no thorough investigation of JM-1232(-)-induced respiratory depression. In the present study, we analyzed the response of the central respiratory activity to JM-1232(-).

I. Homma et al. (eds.), *New Frontiers in Respiratory Control*,
Advances in Experimental Medicine and Biology 669, DOI 10.1007/978-1-4419-5692-7_23,

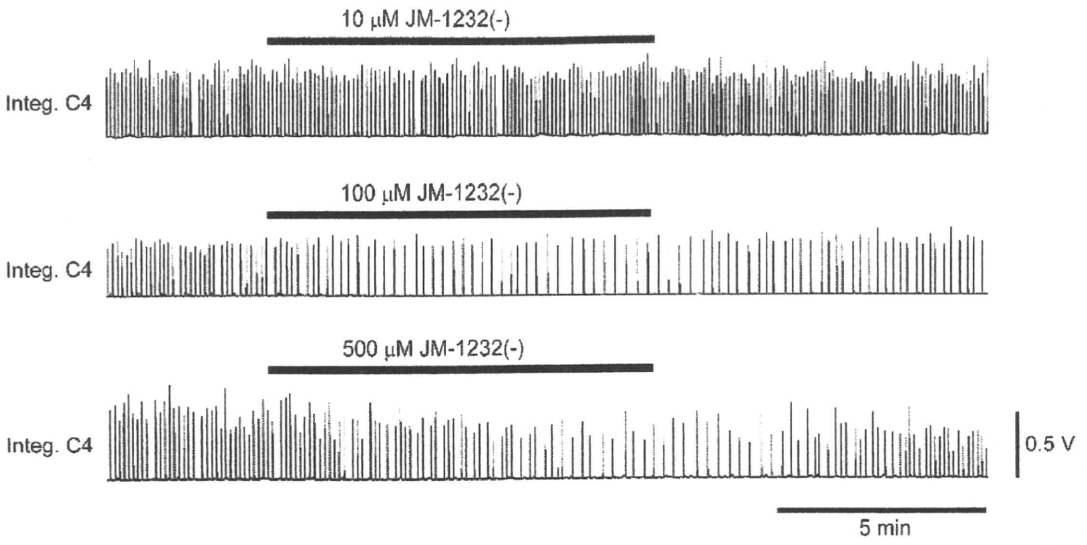

Fig. 1 Representative recordings of the integrated C4 activity (Integ. C4) before, during, and after superfusion with 10, 100 or 500 μM JM-1232(-) The horizontal bars indicate the duration of superfusion with JM-1232(-)

2 Methods

All procedures were conducted in accordance with the institutional guidelines regarding the care of the animals.

Data were obtained from 20 newborn Wistar rats (0–4 days old). Generation of the isolated brainstem-spinal cord preparation has been described in detail elsewhere (Kuwana et al. 1998). In brief, the rats were anesthetized with diethyl ether and the brainstem caudal to the caudal cerebellar artery and cervical spinal cord were isolated in a chamber filled with oxygenated artificial cerebrospinal fluid (ACSF). The cerebellum and pons were ablated. Each preparation was placed ventral side up in a recording chamber (volume, 2 ml) and superfused (flow 4 ml · min^{-1}) with control ACSF equilibrated with a control gas mixture (5% CO_2 in oxygen; pH7.4). Its temperature was maintained at 25–26°C. The composition of the ACSF was (in mM): 126 NaCl, 5 KCl, 1.25 NaH_2PO_4, 1.5 $CaCl_2$, 1.3 $MgSO_4$, 26 $NaHCO_3$ and 30 glucose. C4 ventral root activity was recorded using a glass suction electrode, amplified with a conventional alternating current amplifier (AVH 11, Nihon Kohden, okyo, Japan), and integrated (time constant: 100 m sec). We measured C4 burst rate as an index of the inspiratory rate (Murakoshi et al. 1985) and the integrated amplitude as an index of the tidal volume (Eldridge 1971).

After obtaining the recording with control ACSF, the preparation was superfused with ACSF containing JM-1232(-) (Maruishi Pharmaceutical Co. Ltd., Osaka, Japan) at 10, 100 or 500 μM for 10 min followed by washout for 20–30 min using control ACSF.

Table 1 **Effect of JM-1232(-) on C4 burst activity**

Concentration (μM)	n		Control	JM-1232(-)	Washout
10	6	C4 burst rate (min^{-1})	8.1 ± 1.4	7.9 ± 1.5	7.9 ± 1.4
		C4 burst amplitude (V)	0.50 ± 0.13	0.53 ± 0.13	0.51 ± 0.12
100	8	C4 burst rate (min^{-1})	8.6 ± 2.9	6.4 ± 2.1	9.2 ± 4.1
		C4 burst amplitude (V)	0.55 ± 0.09	0.55 ± 0.09	0.51 ± 0.10
500	6	C4 burst rate (min^{-1})	9.4 ± 1.4	5.4 ± 1.9*	6.8 ± 3.2
		C4 burst amplitude (V)	0.50 ± 0.11	0.47 ± 0.14	0.46 ± 0.14

*$P < 0.01$

All recorded signals were fed into a personal computer after analog/digital conversion (Power Lab/4sp, ADInstruments, Castle Hill, Australia) for subsequent analysis (Chart version 5, ADInstruments, Castle Hill, Australia). Analysis of the respiratory parameters was performed off-line. Respiratory parameters obtained before the superfusion of the ACSF containing drugs were defined as control values. C4 burst rate and amplitude were compared using a one-way analysis of variance, followed by a Dunnett test. All statistical analyses were conducted using Graph-Pad Prism 3.0 software (Graph-Pad Software Inc., San Diego, CA). All values were reported as the mean ± SE and all P values < 0.05 were considered significant.

3 Results

Representative recordings of integrated C4 activity before, during and after superfusion with JM-1232(-) -containing ACSF are shown in Fig. 1. The application of 10 μM JM-1232(-) for 10 min did not decrease C4 burst rate significantly (98 ± 5% of control rate) (Table 1). C4 burst rate slightly decreased by superfusion of ACSF containing 100 μM JM-1232(-) for 10 min (75 ± 8% of control rate), but this decrease was not significant (Table 1). However, the application of 500 μM JM-1232(-) for 10 min significantly reduced C4 burst rate (56 ± 5% of control rate) (Table 1). C4 burst amplitude was not changed by the application of JM-1232(-) for 10 min at any concentrations (Table 1).

4 Discussion

We have demonstrated that the threshold of respiratory depression in JM-1232(-) should lie between 100 or 500 μM.

The peak blood concentration in in vivo rats was 0.78 μM when 0.76 mg JM-1232(-), which corresponds to the hypnotic dose, was given intravenously. Therefore, the peak brain concentration should be lower than 0.78 μM. On the other hand, propofol concentration in the brain tissue of rat in vivo was reported to be approximately 80–200 μM when an anesthetic dose of propofol was given intravenously (Shyr et al. 1995). Thus, the concentration of JM-1232(-) in the brain tissue after the injection of an anesthetic dose may be lower than that of propofol. Conversely, in the

brainstem-spinal cord preparations, only 5 μM propofol induced respiratory depression (Kashiwagi et al. 2004), whereas 500 μM JM-1232(-) only 44% reduction in respiratory rate. Moreover, the application of flumazenil, a benzodiazepine receptor antagonist may reverse JM-1232(-)-induced respiratory depression by the following reasons. First, JM-1232(-) was reported to act through the benzodiazepine site of γ-amino butyric acid type A receptors (Masamune et al. 2009). Second, flumazenil reverse the antinociceptive effect of JM1232(-) (Nishiyama et al. 2008; Chiba et al. 2009). Considering previous report and our results, JM-1232(-) seems to have a wider safety margin in respiratory depression than propofol.

In summary, JM-1232(-) at a low concentration (but presumably higher than hypnotic dose), did not depress the central respiratory activity, whereas at a high concentration depression was seen.

Acknowledgements

This work was Supported by Japan Society for the Promotion of Science KAKENHI (18791106 to Dr. Kuribayashi and 19603015 to Dr. Kuwana), Tokyo, Japan

References

Chiba, S., Nishiyama, T., and Yamada, Y. (2009) The antinociceptive effects and pharmacological properties of JM-1232(-): A novel isoindoline derivative. Anesth. Analg. 108, 1008–1014.

Eldridge, F.L. (1971) Relationship between phrenic nerve activity and ventilation. Am. J. Physiol. 221, 535–543.

Kanamitsu, N., Osaki, T., Itsuji, Y., Yoshimura, M., Tsujimoto, H., and Soga, M. (2007) Novel water-soluble sedative-hypnotic agents: Isoindolin-1-one derivatives. Chem. Pharm. Bull. (Tokyo) 55, 1682–1688.

Kashiwagi, M., Okada, Y., Kuwana, S., Sakuraba, S., Ochiai, R., and Takeda, J. (2004) A neuronal mechanism of propofol-induced central respiratory depression in newborn rats. Anesth. Analg. 99, 49–55.

Kuwana, S., Okada, Y., and Natsui, T. (1998) Effects of extracellular calcium and magnesium on central respiratory control in the brainstem-spinal cord of neonatal rat. Brain Res. 786, 194–204.

Masamune, T., Sato, H., Okuyama, K., Imai, Y., Iwashita, H., Ishiyama, T., Oguchi, T., Sessler, D.I., and Matsukawa, T. (2009) The shivering threshold in rabbits with JM-1232 (-), a new benzodiazepine receptor agonist. Anesth. Analg. 109, 96–100.

Murakoshi, T., Suzue, T., and Tamai, S. (1985) A pharmacological study on respiratory rhythm in the isolated brainstem-spinal cord preparation of the newborn rat. Br. J. Pharmacol. 86, 95–104.

Nishiyama, T., Chiba, S., and Yamada, Y. (2008) Antinociceptive property of intrathecal and intraperitoneal administration of a novel water-soluble isoindolin-1-one derivative, JM 1232 (-) in rats. Eur. J. Pharmacol. 596, 56–61.

Shyr, M.H., Tsai, T.H., Tan, P.P., Chen, C.F., and Chan, S.H. (1995) Concentration and regional distribution of propofol in brain and spinal cord during propofol anesthesia in the rat. Neurosci. Lett. 184, 212–215.

Thyroid Transcription Factor-1 Influences the Early Phase of Compensatory Lung Growth in Adult Mice

Yusuke Takahashi[1,2], Yotaro Izumi[1], Mitsutomo Kohno[1], Tokuhiro Kimura[2], Masafumi Kawamura[1], Yasunori Okada[2], Hiroaki Nomori[1], and Eiji Ikeda[2,3]

[1]Division of General Thoracic Surgery, Department of Surgery, and [2]Department of Pathology, School of Medicine, Keio University, Tokyo, Japan; and [3]Department of Pathology, Yamaguchi University Graduate School of Medicine, Yamaguchi, Japan

Rationale: **Compensatory lung growth has been well described as a phenomenon in many animal models, but still little is known about the nature, extent, and modulation of such growth. We hypothesized that compensatory lung growth may at least in part recapitulate developmental lung growth, and factors known to be important during normal lung development, such as thyroid transcription factor 1 (TTF-1), may be reactivated during compensatory lung growth.**

Objectives: **To investigate the role of TTF-1 in correlation with the morphological changes during compensatory lung growth.**

Methods: **Sequential changes in TTF-1 expression and morphology were examined in the residual right lung after left pneumonectomy in 9-week-old mice. The effect of temporary knockdown of TTF-1 on compensatory lung growth was also evaluated.**

Measurements and Main Results: **TTF-1 was transiently but significantly elevated at an early stage in compensatory lung growth. Morphologically, a process resembling septation in lung development may have been initiated during this period in the vicinity of the alveolar duct. Furthermore, temporary knockdown of TTF-1 transiently but significantly delayed the early phase of compensatory lung growth.**

Conclusions: **These results indicate the influential role of TTF-1 in modulating, and possibly initiating, the early phase of compensatory lung growth. Morphologically, compensatory lung growth may at least in part resemble developmental growth.**

Keywords: thyroid transcription factor 1; septation; alveolar duct

Lung resection continues to be the primary treatment for many types of lung diseases, including cancer and inflammatory lung diseases. One of the most important factors that determine the level of resectability is the residual lung function. We know clinically that after lung resection in adults the residual lung increases in volume to some extent, but this is considered to be primarily hyperinflation with minimal recovery and possibly even deterioration in lung function (1). On the other hand, in children, recovery in lung function after lung resection has been reported (2). It is well established that alveoli multiply after birth up until about 8 years of age (3), and in addition, adult lungs transplanted into immature recipients have been reported to show hyperplastic growth (4). These results suggest that it may be possible, at least in part, to restore or augment compensatory growth capability even in adult lungs.

Compensatory lung growth after lung resection has been reported in many animal models, including mice (5, 6). Compensatory lung growth has been well described as a phenomenon, but still little is known about the nature, extent, and modulation of such growth. The involvement of multiple factors, such as epidermal growth factor (7), hepatocyte growth factor (8), keratinocyte growth factor (9), and vascular endothelial growth factor (10), has been implicated in compensatory lung growth, but what triggers and what drives compensatory lung growth is still not clear. Although still controversial, it has been postulated that compensatory lung growth may at least in part recapitulate developmental lung growth (11). If so, compensatory lung growth may occur via partial reactivation of normal developmental pathways, and factors known to be important during normal lung development, such as thyroid transcription factor 1 (TTF-1), may be reactivated during compensatory lung growth. The reported reappearance of TTF-1 in regions of regenerating lung after lung injury supports the possibility that TTF-1 plays a role in alveolar cell growth and differentiation and that TTF-1 may be a critical factor in the restoration of alveolar structures that accompanies recovery from functional loss after lung diseases or lung injury (12).

To our knowledge, the role of TTF-1 in compensatory lung growth has not been closely investigated. In the present study, we show that TTF-1 expression was transiently elevated at an early stage in compensatory lung growth and that morphologically, a process resembling septation during lung development may have been initiated during this period in the vicinity of the alveolar duct. Furthermore, temporary knockdown of TTF-1 delayed the early phase of compensatory lung growth, indicating its influential role in modulating and possibly initiating the early phase of compensatory lung growth.

AT A GLANCE COMMENTARY

Scientific Knowledge on the Subject

Compensatory lung growth has been well described in many animal models as a phenomenon, but still little is known about the nature, extent, and modulation of such growth.

What This Study Adds to the Field

Here we show that expression of thyroid transcription factor 1, a factor known to be indispensable in normal lung development, significantly influences the early phase of compensatory lung growth in adult mice, and that morphologically, a process resembling septation in lung development may be initiated during this period in the vicinity of the alveolar duct.

METHODS

Animal Experiments

Specific pathogen-free, 9-week-old, inbred male C57BL/6 mice, weighing approximately 20 g, were purchased from CLEA Japan, Inc. (Tokyo,

(Received in original form August 21, 2009; accepted in final form February 24, 2010)

Supported by grant in aid from the Ministry of Education, Culture, Sports, Science, and Technology–Japan, and the School of Medicine, Keio University fund for the promotion of science.

Correspondence and requests for reprints should be addressed to Eiji Ikeda, M.D., Ph.D. Department of Pathology, Yamaguchi University Graduate School of Medicine, 1-1-1 Minami-Kogushi, Ube, Yamaguchi 755-8505, Japan. E-mail: ikedae@yamaguchi-u.ac.jp

Am J Respir Crit Care Med Vol 181. pp 1397–1406, 2010
Originally Published in Press as DOI: 10.1164/rccm.200908-1265OC on March 1, 2010
Internet address: www.atsjournals.org